Curr Radiol Rep (2015) 3:19
DOI 10.1007/s40134-015-0100-5

Advances in Lower Extremity Ultrasound

Mihra S. Taljanovic[1] · David M. Melville[1] · Andrea S. Klauser[2] · Leonard Daniel Latt[3] · Hina Arif-Tiwari[1] · Liang Gao[4] · Russell S. Witte[4]

Published online: 21 April 2015

Abstract Diagnostic ultrasound techniques used in the evaluation of the musculoskeletal system are rapidly evolving. Conventional B-mode and Doppler ultrasound imaging methods are workhorses in the diagnosis and treatment decision making for traumatic and pathologic conditions of joints, tendons, muscles, ligaments, and peripheral nerves. Recently developed sonoelastography techniques enable the qualitative and quantitative evaluation of the material properties of musculoskeletal tissues. The recent availability of sonoelastography on clinical machines will facilitate its progressive utilization in routine clinical practice. Exciting new developments in ultrasound imaging enable real-time fusion with imported magnetic resonance or computed tomography images, facilitating ultrasound-guided interventional procedures and teaching of ultrasound anatomy to trainees. In this review article, the authors discuss new advances in sonoelastography of the lower extremity with emphasis on shear wave imaging and briefly the exciting features of ultrasound fusion imaging with computed tomography and magnetic resonance imaging.

Keywords Lower extremity · Ultrasound · Advances · Sonoelastography · Ultrasound elasticity imaging · Ultrasound elastography

Introduction

During the past two decades, ultrasound (US) is being increasingly used in the diagnosis of various musculoskeletal injuries and diseases of the lower extremities with results comparable to magnetic resonance (MR) imaging [1]. US has been routinely used in the diagnosis and follow-up of developmental dysplasia of the infant hip for three decades [2]. This imaging modality is frequently used to guide aspiration of the joint effusions and soft tissue fluid collections, as well as perform therapeutic injections, and soft tissue biopsies of the musculoskeletal system including the

This article is part of the Topical Collection on *Musculoskeletal Ultrasound*.

✉ Mihra S. Taljanovic
mihrat@radiology.arizona.edu

David M. Melville
dmelville@radiology.arizona.edu

Andrea S. Klauser
andrea.klauser@i-med.ac.at

Leonard Daniel Latt
dlatt@email.arizona.edu

Hina Arif-Tiwari
hinaarif@radiology.arizona.edu

Liang Gao
lgao@email.arizona.edu

Russell S. Witte
rwitte@radiology.arizona.edu

[1] Department of Medical Imaging, The University of Arizona Health Network, 1501 N. Campbell Ave., P.O. Box 245067, Tucson, AZ 85724, USA

[2] Section Rheumatology and Sports Imaging, Department of Radiology, Medical University Innsbruck, Anichstrasse 35, 6020 Innsbruck, Austria

[3] Department of Orthopaedic Surgery, The University of Arizona Health Network, 1501 N. Campbell Ave., P.O. Box 245064, Tucson, AZ 85724, USA

[4] Medical Imaging, Biomedical Engineering, Optical Sciences, University of Arizona, 1609 N Warren Ave, Bldg 211, Rm 124, Tucson, AZ 85724, USA

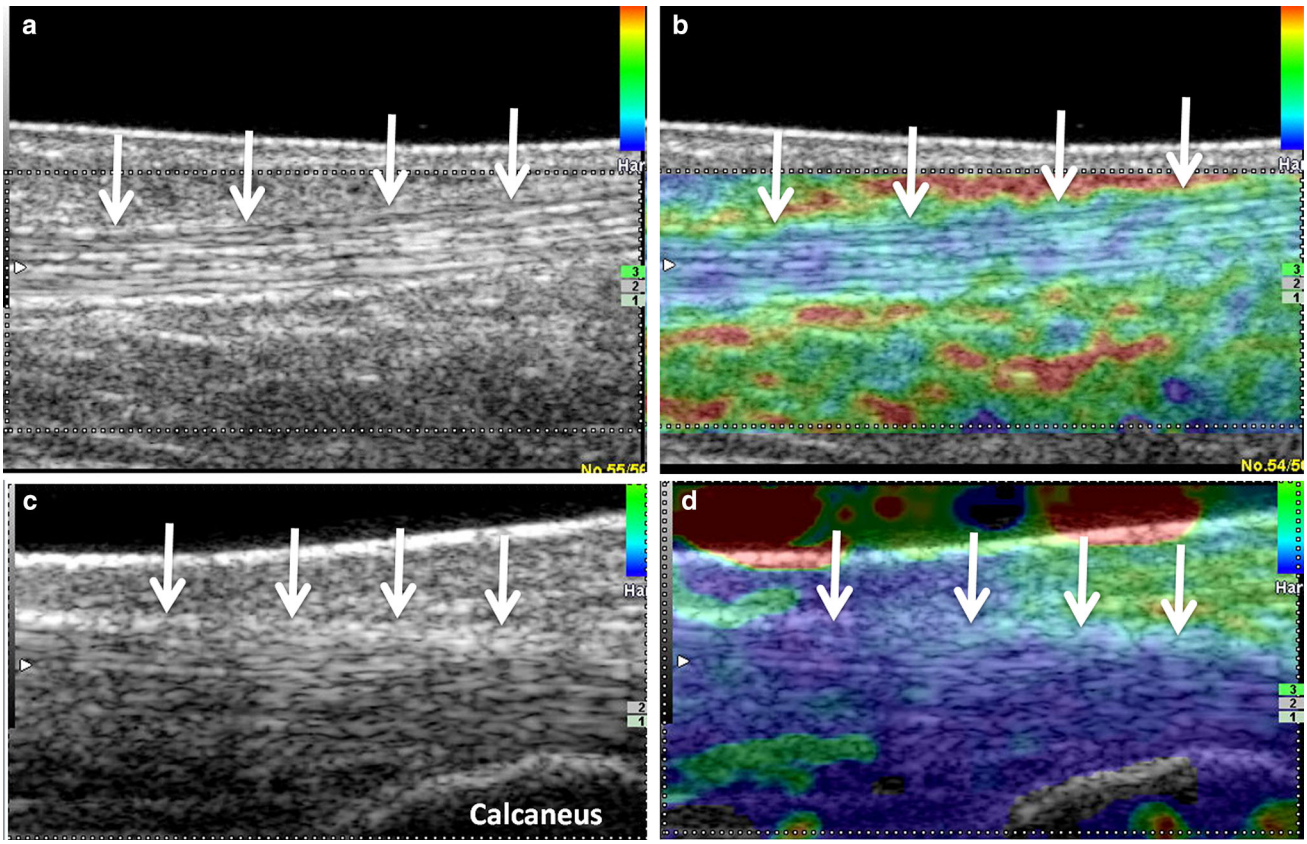

Fig. 1 B-mode (*grayscale*) and compression SEL images of a normal Achilles tendon (*arrows*). Long-axis grayscale images of the middle (**a**) and distal (**c**) Achilles tendon reveal normal echogenic fibrilar echotexture. Long-axis elastograms of the middle (**b**) and distal (**d**) Achilles tendon reveal blue and green color within the tendon consistent with hard/stiff tissue. *Red* color is defined for encoding soft consistency, *blue* and *green* indicate hard consistency, and the *yellow* color encodes the intermediate stiffness. Images obtained on HI VISION Preirus US machine, Hitachi Aloka Medical, Ltd, Tokyo, Japan with 5-18-MHz linear array transducer (Color figure online)

lower extremity [3]. US is also used to guide therapeutic tendon fenestration with and without platelet-rich plasma or autologous blood injection [4–6]. Dynamic real-time imaging is frequently used to diagnose extra-articular snapping hip including the external causes (e.g., snapping iliotibial band or gluteus maximus) and the internal causes (e.g., snapping iliopsoas tendon) [7, 8]. US is gaining popularity in evaluation of the pseudotumors associated with metal-on-metal hip arthroplasty [9, 10]. Color and power Doppler imaging adds valuable information related to vascularity of the examined tissue [11].

However, it may be difficult to distinguish pathological from healthy tissue during a conventional US exam because they often display similar echogenicities. In recent years, sonoelastography (SEL) was introduced as a new technique to help in the evaluation of soft tissue elasticity in addition to information obtained by conventional US. In particular in the musculoskeletal system, SEL may be useful in depicting soft tissue edema, early tendinopathy, or small partial-thickness tears that may be isoechoic to surrounding healthy tissues on conventional US. There are three main types of SEL including compression SEL (Fig. 1), transient elastography (TE), and shear wave elastography (SWE) (Figs. 2, 3, 4, 5, 6, 7), each with advantages and disadvantages [12, 13].

Basic Technical Principals of Sonoelastography

Static Elastography

Static SEL enables visualization of tissue displacement and strain in real-time in response to an applied or internal force (stress) [14]. Strain is defined as a change in size or shape and can be expressed mathematically as a ratio of the change in length per unit length. Displacement and strain between frames are estimated at each pixel using a speckle tracking algorithm with advanced signal processing techniques. Strain is less for harder tissues. In the "freehand SEL" compression technique, which is commercially available on most modern US machines, tissue strain is generated by the application of light pressure to the skin,

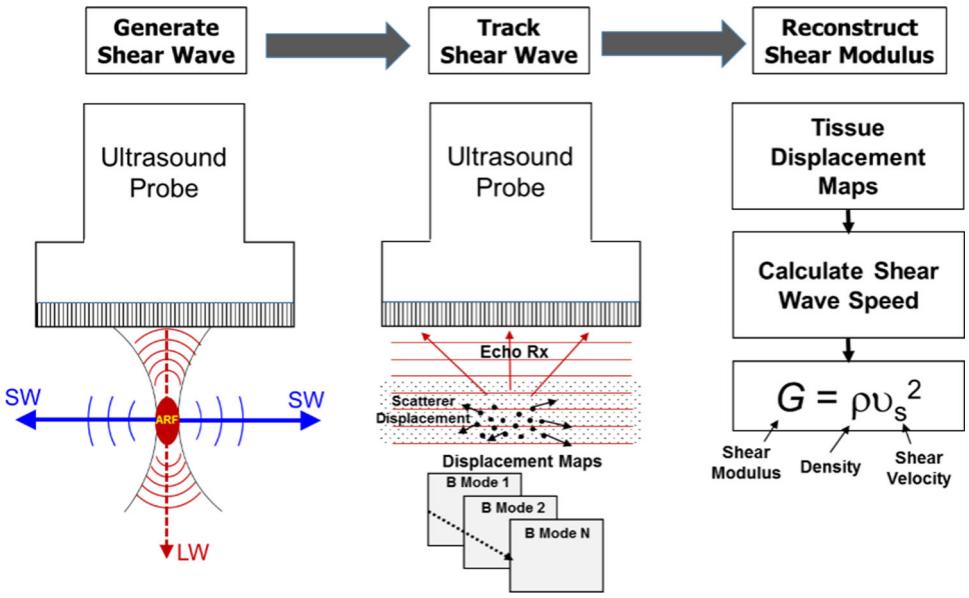

Fig. 2 *Left* generation of shear waves (SW) using an acoustic radiation force pulse sequence. SWs propagate perpendicular to the longitudinal wave at a much slower velocity. *Middle* high frame rate plane wave excitation is used to track the displacement and velocity of the tissue as the SWs propagate. Displacements between frames in the tissue are calculated using a speckle tracking algorithm. *Right* the displacements are converted to velocities to determine shear wave speed and conversion to an elastic (shear or Young's) modulus according to the mathematical equation

while the system displays a grayscale image of the tissue strain alongside the conventional US image. Alternatively, these two images may be combined by overlaying conventional US with color-coded SEL for enhanced tissue contrast. The standard color images (elastograms) progress from soft (red), intermediate (yellow), to hard (green and blue). However, the dynamic range of the color map can be adjusted by the user (Fig. 1). The majority of these systems display the applied pressure and also a semiquantitative measurement of the strain ratio, which is an index of the relative elasticity between a chosen region of interest (ROI) in the examined tissue and a reference ROI usually in the adjacent subcutaneous tissues [12, 13]. Disadvantages of static compression SEL include operator dependence, limited reproducibility, and availability of only qualitative information [12, 13]. An additional limitation of static compression SEL is the so-called "egg shell" effect in which the harder outer tissues of a lesion cannot be deformed, limiting the assessment of internal tissue strains [15, 16]. When performing static SEL, the US transducer should be perpendicular to the examined structure to achieve an optimal linear compression force and accurate measure of tissue elasticity [13, 17]. Additional pitfalls in static SEL include the possibility of inaccurate elastograms at the beginning and end of each pressure cycle and an inhomogeneous compression force at the edge of the transducer, especially in the transverse plane. Therefore, the examined tissue should be in the center of the elastogram window to enable a more uniform compression [12]. Stand-off pads may be used to adjust for the shallow depth of superficial structures less than 5 mm from the skin surface [18].

Tension elastography is another type of static SEL in which tissue strain is measured in response to an internally generated tensile stress. This approach has recently been applied to human tendon [19•]. The tensile force is created by the voluntary isometric contraction of muscle, while the magnitude of the force is measured externally using a dynamometer. In contrast to compression SEL, this technique does provide quantitative information. Tension SEL is particularly useful for evaluation of tendons because their function is to transmit tensile force from muscle to bone. Although this technique is not yet commercially available, it holds great promise as a new functional imaging test of tendon, which may help guide treatment for tendinopathy [19•].

Dynamic Elastography and Shear Wave Elastography (SWE)

Dynamic elastography involves measuring the velocity of shear waves generated by either an external vibrator (transient elastography [TE]) or an acoustic radiation force pulse. With TE, low-frequency (~50–60 Hz) vibrations at the skin surface generate propagating shear waves in the tissue. The local velocity of the shear waves (typically from 1 to 10 m/s) is directly related to the local Young's modulus. However, TE enables only regional measurement of tissue elasticity with limited depth. For accurate measurement, the depth of the ROI should be set between 35 and 75 mm from the skin surface [12, 13].

For acoustic radiation force imaging (ARFI), a focused US radiation force produces a local deformation at the ROI, generating a shear wave that propagates perpendicular to the longitudinal wave (see Fig. 2, left) [20, 21]. The sequence of steps from generating and tracking the shear waves to computing the shear moduli is depicted in Fig. 2. The tissue elasticity is typically measured in

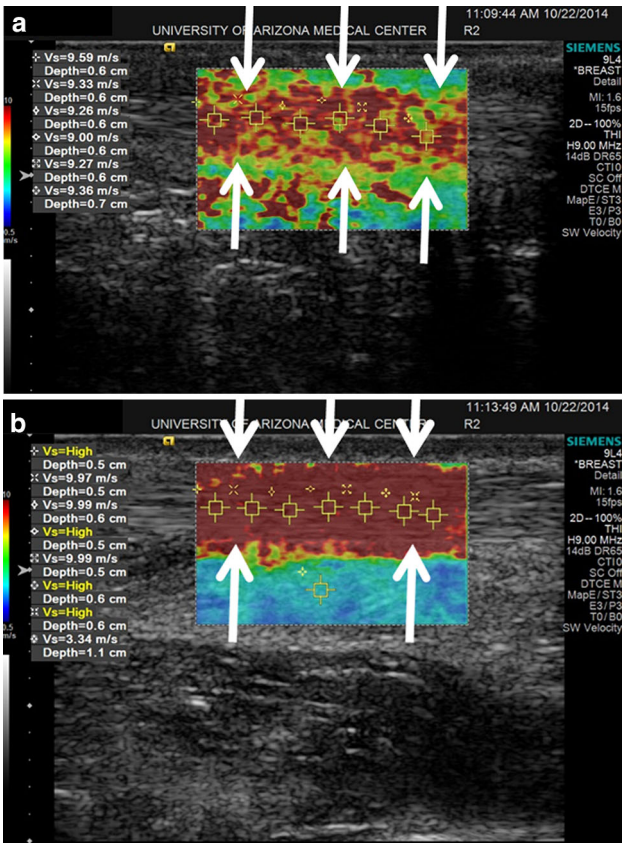

Fig. 3 Long-axis SWE images of the (**a**) relaxed and (**b**) contracted Achilles tendon (*arrows*) in an asymptomatic volunteer show increased tendon stiffness with some increased velocity with contraction. *Red* color is defined for encoding hard consistency, *blue* and *green* indicate soft consistency, and the *yellow* color encodes the intermediate stiffness. Images obtained on Siemens Acuson S-3000 US machine with L9-4-MHz linear transducer (Color figure online)

kilopascals (kPa). Young's modulus (E) represents the ratio of stress to strain and can be calculated directly from the shear wave velocity (v_s) and material density (ρ) according to the equation $E = 3\rho v_s^2$. Therefore, shear waves propagate faster in harder tissues and the distribution of shear wave velocities at each pixel is directly related to the shear modulus. Quantitative Young's modulus maps are represented in color (elastograms) displaying tissue elasticity (in kPa) or shear wave velocity (in m/s) [21]. SWE is considered to be more objective, quantitative, and reproducible than static SLE. Because the shear waves in soft tissue travel about a thousand times slower than longitudinal waves, US images can be used to compute the shear wave velocity as long as the US frame rate is high enough. Frame rates typically exceed 1 kHz, enabling real-time visualization of shear waves propagating in biological tissues, conveying local information about elastic and viscoelastic tissue properties. Disadvantages of the currently available SWE measurements are the limitation of the depth of tissue penetration and limited shapes and sizes of the ROI (small regions of interest measuring only a few mm) [20, 21]. To facilitate imaging at shallower depths, coupling gel or a stand-off pad can be used while performing SWE.

Figures 3, 4, 5, 6, and 7 are examples of ARFI SWE obtained in first author's institution on Siemens Acuson S-3000 US machine with L9-4-MHz linear transducer. Figure 3 shows SWE of a normal Achilles tendon in the relaxed and contracted states and Fig. 4, SWE of a relaxed and contracted Achilles tendon in a symptomatic patient with tendinopathy. Figure 5 demonstrates SWE of a relaxed and contracted normal gastrocnemius/soleus muscle unit. Figure 6 shows SWE of a normal neurovascular bundle in the tarsal tunnel and Fig. 7, SWE of a normal plantar fascia. The color bar indicates the velocity of the shear wave (from 0.5 m/s [blue] to 10 m/s [red]).

Sonoelastography (SEL) of the Lower Extremity Soft Tissues

Static Sonoelastography

Several studies have been published on utility of compression SEL of the lower extremity musculoskeletal structures with promising results [22–31]. The majority of clinical studies focused on Achilles tendon [22–26] with a limited number of publications related to other anatomic structures including patellar tendon [27], plantar fascia [28], and the skeletal muscle [29, 30].

De Zordo and collaborators examined Achilles tendons in 25 consecutive patients with chronic Achilles tendinopathy and 25 healthy volunteers by clinical exam, conventional US, and compression SEL. In this study, 93 % of Achilles tendons of healthy volunteers were hard, while 57 % of tendons in the patients were soft. Mild softening was found in 7 % of the healthy volunteers and in 11 % of the patients. With the clinical examination used as a reference standard, the mean sensitivity, specificity, and accuracy of SEL were 94, 99, and 97 %, respectively. The correlation to conventional US was 0.89. The authors concluded that only distinct softening of Achilles tendons is comparable to clinical examination and conventional US findings, and the mild softening on SEL could be explained by very early changes in tissue elasticity in the case of developing Achilles tendinopathy [22]. In another SEL study on 80 asymptomatic Achilles tendons (divided in 3 thirds/240 regions) in 40 volunteers by De Zordo and collaborators, 86.7 % of the tendons were hard, 12.1 % showed mild softening, and 1.3 % (3/240) showed distinct softening, which correlated with B-mode US imaging to indicate subclinical stage of disease [23].

Drakonaki and collaborators performed free-hand compression SEL of 50 Achilles tendons in asymptomatic

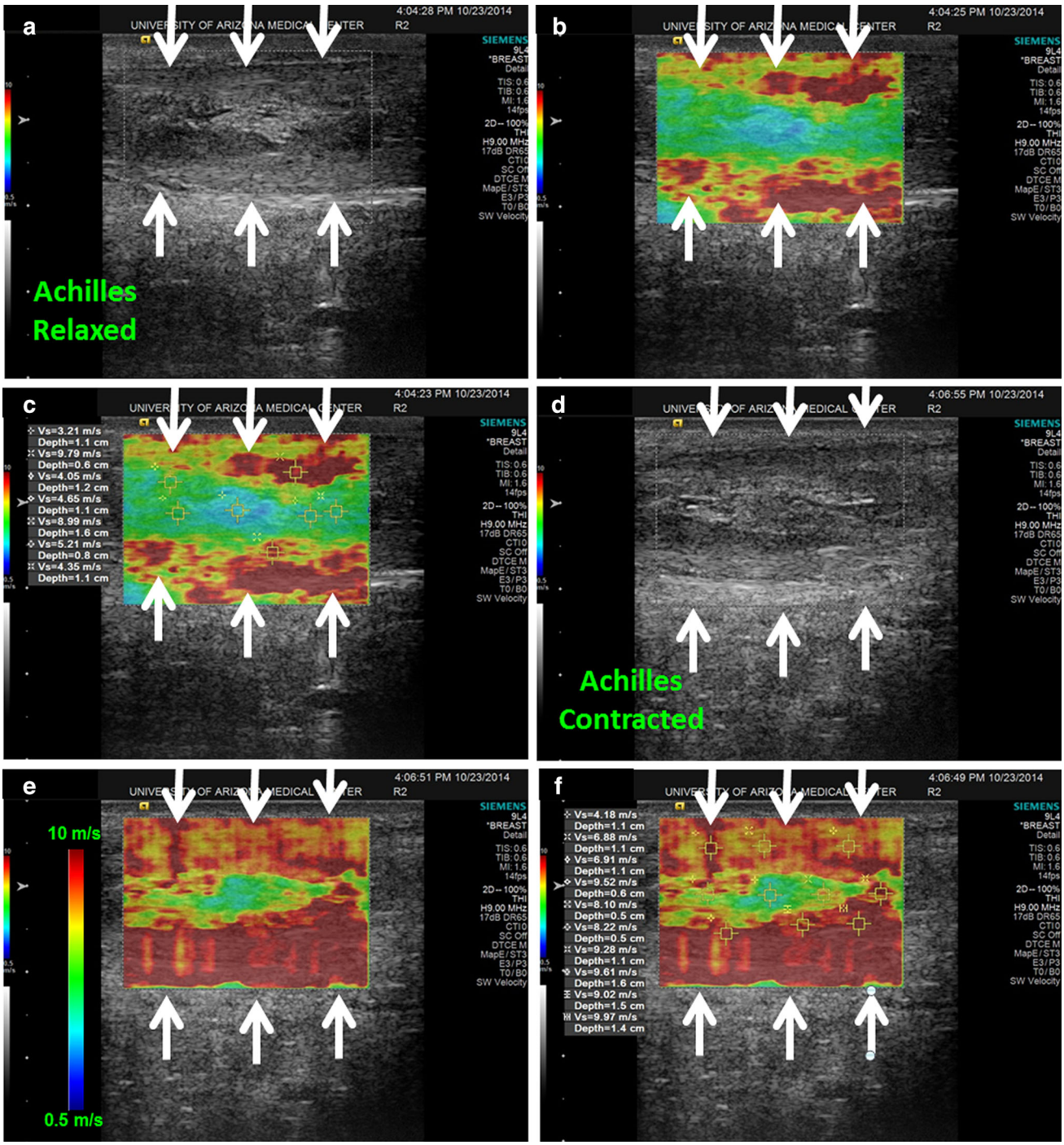

Fig. 4 Long-axis *grayscale* and SWE images of the relaxed (**a**–**c**) and contracted (**d**–**f**) Achilles tendon (*arrows*) in a symptomatic patient with severe tendinopathy. *Grayscale* images (**a**, **d**) show fusiform thickening of the middle part of the Achilles tendon which is heterogeneous with partial loss of a normal fibrilar echotexture. On the SWE images (**b**, **c**, **e**, **f**) note central tendon softening with decreased velocity (*blue* and *green* colors) compared to hardest consistency with higher velocities at the tendon periphery. With contraction (**e** and **f**) the central part of the tendon remains soft. Images obtained on Siemens Acuson S-3000 US machine with L9-4-MHz linear transducer (Color figure online)

individuals to evaluate for intra- and inter-reader reproducibility. Two radiologists examined each tendon three times transversely and longitudinally, and the ratio between tendon and retro-Achilles fat strain (strain index) was calculated. In this study, the reproducibility of the strain index was good and higher for longitudinal elastograms

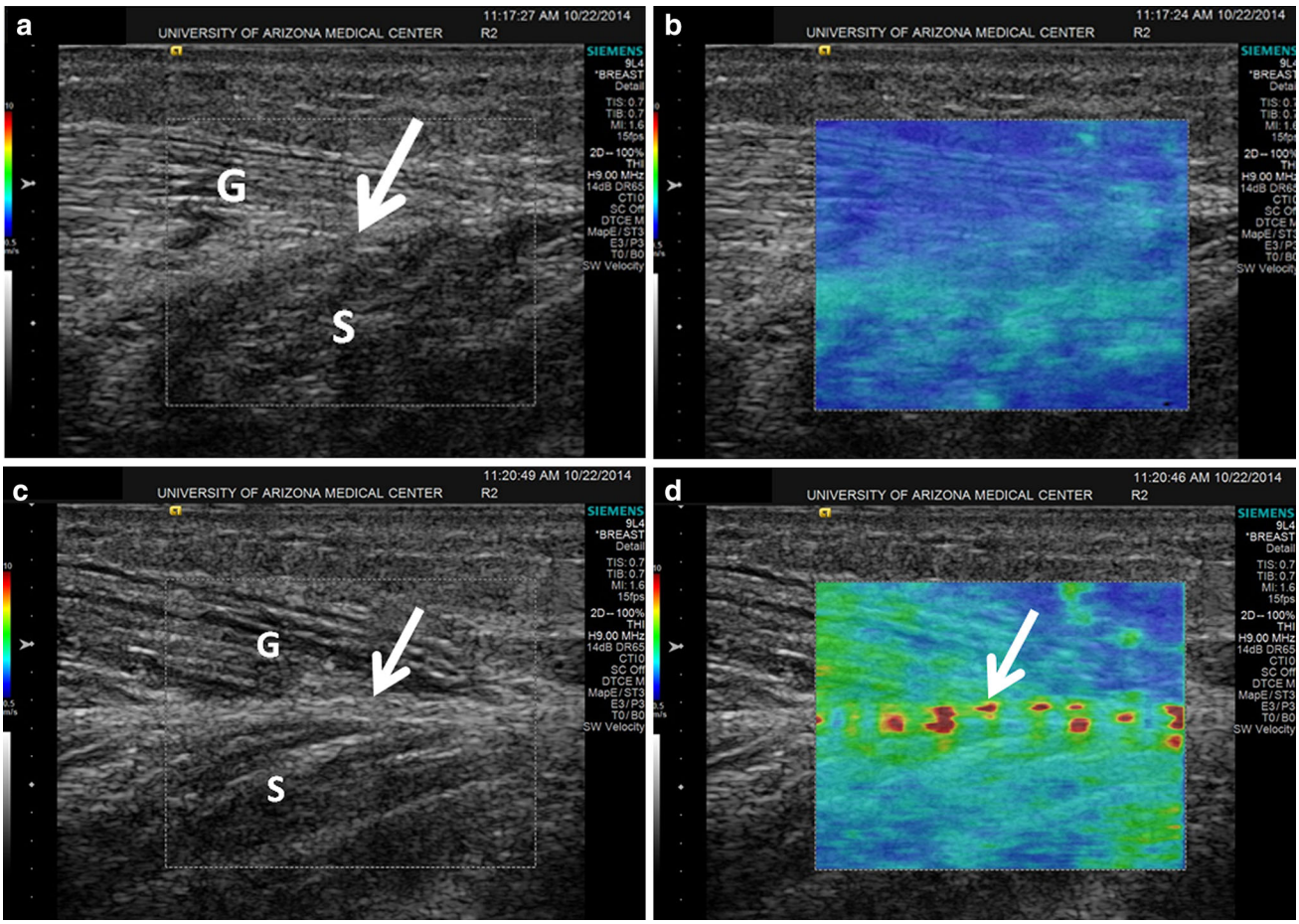

Fig. 5 Long-axis *grayscale* (**a** and **c**) and SWE (**b** and **d**) images of the medial head of gastrocnemius muscle/soleus aponeurosis with relaxed (**a** and **b**) and contracted muscles (**c** and **d**) in an asymptomatic volunteer. Normal hypoechoic muscular echotexture with hyperechoic septa and aponeurosis (*arrow*) is seen on the *grayscale* (**a** and **c**) images. In (**b**), note *blue* color in the SWE window related to soft consistency with low velocity. With muscular contraction (**d**), there is increased stiffness and velocity, mostly in the region of the aponeurosis (*arrow*). *G* gastrocnemius muscle, *S* soleus muscle. Images obtained on Siemens Acuson S-3000 US machine with L9-4-MHz linear transducer (Color figure online)

and the qualitative assessment enabled the discrimination of two distinct elastographic patterns. Nineteen of 50 tendons (38 %) appeared homogeneously green/blue (designated as type 1), while 39 tendons (62 %) were green with longitudinal red stripes (designated as type 2) without corresponding abnormality on B-mode or Doppler ultrasound evaluation [24].

Tan and collaborators evaluated compression SEL appearance of the proximal, middle, and distal thirds of 19 surgically repaired Achilles tendons in 16 amateur soccer players, in their asymptomatic contralateral Achilles tendons, and of additional 40 asymptomatic Achilles tendons of 20 healthy amateur soccer players. The tendons were graded 1–3 (type 1—blue—hardest tissue, type 2—blue/green—hard tissue, and type 3—green—intermediate tissue) and additionally classified as homogeneous, relatively homogeneous, and heterogeneous. The majority (64.9 %) of surgically repaired ruptured Achilles tendons were hard with type 2 elasticity, while the remainder had type 1 elasticity. The majority of healthy tendons had type 2 (64.2 %), and the remaining had either a type 3 (20.8 %) or a type 1 (15 %) elasticity. All repaired ruptured tendons were heterogeneous, while the healthy Achilles tendons had homogeneous or relatively homogeneous pattern [25].

Klauser and collaborators compared B-mode US imaging and compression SEL examinations of 13 cadaveric Achilles tendons with histologic correlation. On conventional US, the tendons were graded 1–3 [(1) normal size and fibrillar echotexture, (2) focal fusiform enlargement, or (3) a hypoechoic area with or without tendon enlargement). On SEL, grade 1 indicated blue (hardest) to green (hard); grade 2, yellow (soft); and grade 3, red (softest) tendon. In this study, the SEL findings were concordant in all cases of histologic degeneration, whereas B-mode US alone showed two false-negative findings in 14 % of cases [26].

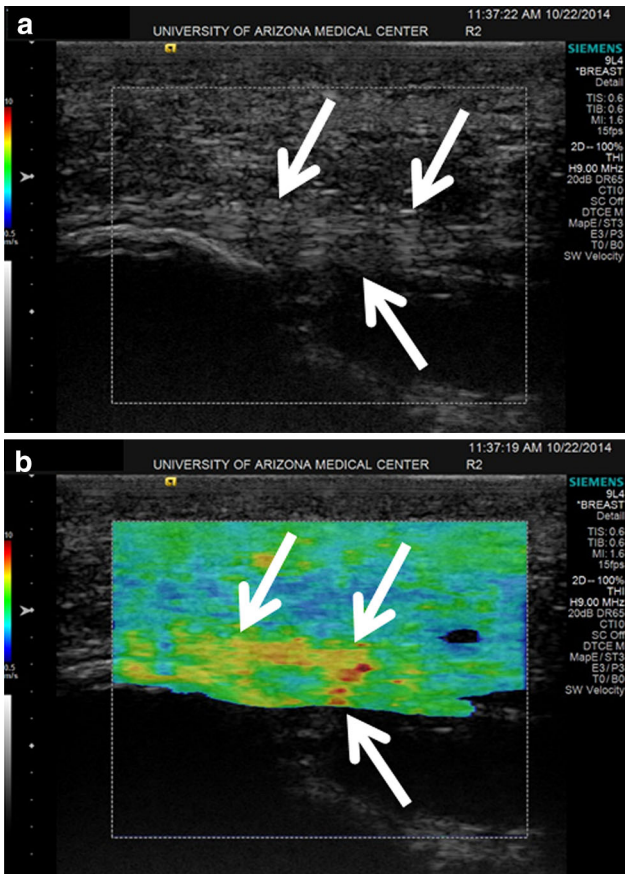

Fig. 6 Long-axis *grayscale* (**a**) and SWE (**b**) images of the proximal plantar fascia (*arrows*) in an asymptomatic 36-year-old man show normal echotexture in (**a**) with predominantly intermediate fascial stiffness in (**b**). Images obtained on Siemens Acuson S-3000 US machine with L9-4-MHz linear transducer

In a study by Rist and Mauch on 37 asymptomatic and 38 symptomatic patellar tendons in athletes, symptomatic tendons with associated tendinopathy had significantly higher strain scores in the longitudinal and transverse sections semiquantitative measurements [27].

Wu and collaborators performed color-coded compression SEL on bilateral feet of 40 healthy subjects and 13 subjects with plantar fasciitis. Healthy subjects were divided into two groups, including those younger than 50-year old and older than 50-year old. In this study, the SEL revealed that the plantar fascia softens with age and in subjects with plantar fasciitis [28].

In a case report of a 15-year old with Bethlem muscular dystrophy, the hyperechoic regions at the muscle periphery and the central parts of the affected muscles were harder on compression SEL when compared to the normal appearing muscle parts. The authors concluded that the abnormal findings probably correlate with the presence of dystrophic collagen at the affected areas and suggested that the compression SEL may be of value to evaluate the pattern of muscle changes in congenital myopathy [29].

Vasilescu and collaborators performed compression SEL in 7 children with cerebral palsy spasticity to find the proper place for injecting the botulinum toxin (20 U/kg Dysport) into the affected muscle. The relaxed muscle structures appear mostly soft (green–yellow–red), while contracted or degenerated muscle fibers appear hard (blue). This technique enabled a precise, guided injection, with positive, therapeutic results [30].

At present, there is a paucity of literature addressing the SEL evaluation of the lower extremity nerves. A case report of a common peroneal nerve schwanoma revealed a well-defined hypoechoic inhomogeneous eccentrically located mass in continuity with the common peroneal nerve, which showed a strong inhomogeneous enhancement after intravenous administration of ultrasound contrast agent. Compression SEL in the affected region revealed the presence of a hard solid mass, which was much harder than the surrounding skeletal muscles. The US findings correlated with the MR imaging study [31].

Dynamic Elastography and Shear Wave Elastography (SWE)

There are a few published human studies on SWE of the musculoskeletal soft tissues of the lower extremities including tendon [32, 33•, 34–36] and muscle [32, 37, 38, 39•].

To determine the baseline values of different healthy tissues, Arda and collaborators examined the gastrocnemius, masseter and supraspinatus muscles, and the Achilles tendon of 127 healthy volunteers of both genders (age range 17–63 years) with SWE in both longitudinal and transverse planes using a 13–6-MHz linear array transducer (R 3.2, Supersonic Imaging System). The mean elasticity values for the gastrocnemius, masseter and supraspinatus muscles, and the Achilles' tendon in both longitudinal and transverse planes were 11.1 ± 4.1 kPa (range, 2–28 kPa) for the gastrocnemius muscle in men and 11.1 ± 4.0 kPa (range 4–26 kPa) in women, 10.8 ± 3.9 kPa (range 4–20 kPa) for the masseter muscle in men and 10.3 ± 3.6 kPa (range 2–23 kPa) in women, 36.0 ± 13.0 kPa (range 11–77 kPa) for the supraspinatus tendon in men and 29.1 ± 12.4 kPa (6–90 kPa) in women, 98.8 ± 47.1 kPa (range 8–242 kPa) for the longitudinal plane of the Achilles tendon in men and 62.5 ± 40.1 (range 6–176) in women, and 51.1 ± 23.8 kPa (range 15–98 kPa) for the transverse plane of the Achilles' tendon in men and 51.7 ± 25.7 kPa (range 10–111 kPa) in women. The mean elasticity values for the examined musculature and the Achilles' tendon in the longitudinal plane were greater in men than in women, but there was no statistically significant difference for the elasticity of the Achilles tendon in transverse plane between men and women. There was no statistically significant positive or

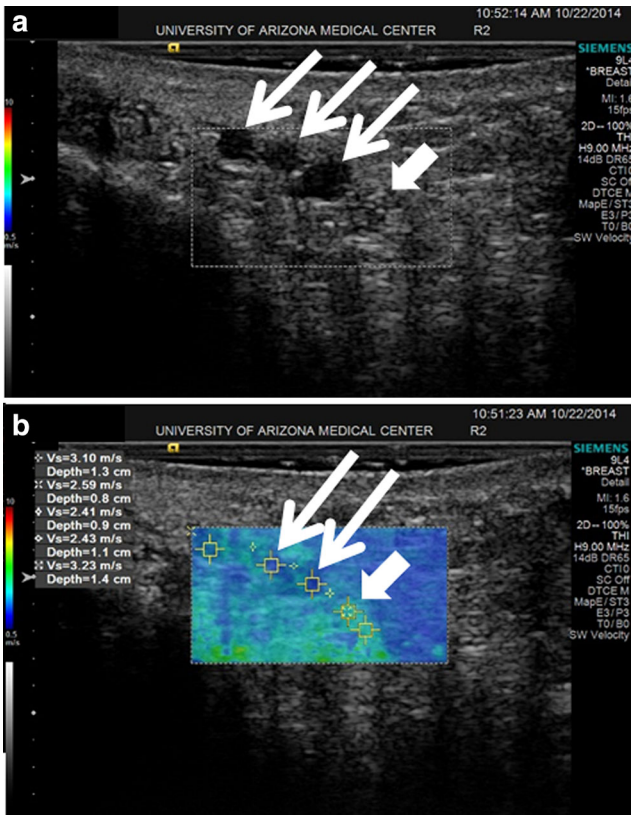

Fig. 7 Short-axis *grayscale* (**a**) and SWE (**b**) images of a tarsal tunnel in an asymptomatic volunteer show in (**a**) normal anechoic echotexture of the tibial posterior artery and veins (*arrows*) and normal honeycomb appearance of the tibial posterior nerve (*thick arrow*). In (**b**), note *blue* color in the posterior tibial vessels and *green* in the nerve indicating somewhat harder consistency and higher velocity in the nerve (*thick arrow*) compared to adjacent vessels (*arrows*). Images obtained on Siemens Acuson S-3000 US machine with L9-4-MHz linear transducer (Color figure online)

negative correlation between the elasticity of the examined muscles or the Achilles tendon and subject's age [32].

DeWall and collaborators investigated spatial variations in Achilles tendon shear wave speed from the calcaneus insertion to the medial and lateral gastrocnemius aponeuroses in ten asymptomatic volunteers in resting position, and plantar and dorsiflexion. US B-mode images and shear wave data were collected using an Aixplorer clinical machine (Supersonic Imagine; Aix-en-Provence, France; software version 5) with a 15-4-MHz linear array transducer. The results of this study showed that shear wave speed is closely linked to the spatial position along the Achilles tendon, varies between the medial and lateral sides, and depends directly on ankle posture. These observations demonstrated the critical importance of considering both spatial location and posture when using SWE for biomechanical or clinical evaluations of the Achilles tendon. Shear wave speeds in the Achilles free tendon averaged 12 ± 1.2 m/s in a resting position, but decreased to 7.2 ± 1.8 m/s with passive plantar flexion. Distal tendon shear wave speeds often reached the maximum tracking limit (16.3 m/s) of the system when the ankle was in the passively dorsiflexed posture. At a fixed posture, shear wave speeds decreased significantly from the free tendon to the gastrocnemius myotendionous junction, with slightly higher speeds measured on the medial side than on the lateral side. Shear wave speeds were only weakly correlated with the thickness and depth of the tendon, suggesting that the distal-to-proximal variations may reflect greater compliance in the aponeurosis relative to the free tendon [33•].

Chen and collaborators studied 36 normal and 14 ruptured Achilles tendons with SWE using an Aixplorer US machine (Supersonic Imagine; Aix-en-Provence, France; software version 5) with 15-4-MHZ linear array transducer. In this study, the normal Achilles tendons were significantly stiffer when compared with the ruptured tendons. The authors concluded that SWE is a valuable tool that can provide complementary biomechanical information for evaluating the function of the Achilles tendon [34].

Aubry and collaborators performed conventional US and SWE studies on 180 asymptomatic and 30 symptomatic Achilles tendons in the mid portion in both long and short axes using a US system (Aixplorer; SuperSonic Imagine, Aix-en-Provence, France) equipped with a 12-MHz linear transducer. In this study, SWE revealed significant softening of the mid portion of the Achilles tendon in patients with tendinopathy, in both relaxed and stretched tendons. The elastographic anisotropy was not altered by tendinopathy. With relaxed Achilles tendon (full passive plantar flexion), tendon softening was characterized by mean velocity of 4.06 m/s at axial SWE with high specificity of 91 % and low sensitivity of 54.2 %, and with stretched Achilles tendon (0° flexion), tendon softening was characterized by a mean velocity of less than or equal to 4.86 m/s at axial SWE or less than or equal to 14.58 m/s at sagittal SWE, which were indicators of mid portion tendinopathy. SWE revealed signal voids in the region of Achilles tendon partial-thickness tears [35].

Recent grayscale and SWE study in 33 male athletes (20 with asymptomatic patellar tendons and 13 with unilateral proximal patellar tendinopathy) revealed a stiffer and larger tendon on the painful side with patelar tendinopathy when compared to the non–painful side and the dominant side of healthy athletes. The data were collected using an Aixplorer US machine (Aixplorer; SuperSonic Imagine, Aix-en-Provence, France) with a 15-MHz linear array transducer. No significant differences of patellar tendon morphology and elastic properties were detected between the dominant and non-dominant knees of the healthy control. A higher shear elastic modulus ratio, with greater differences between the painful and non-painful tendon, was associated with greater intensity of pain with pressure.

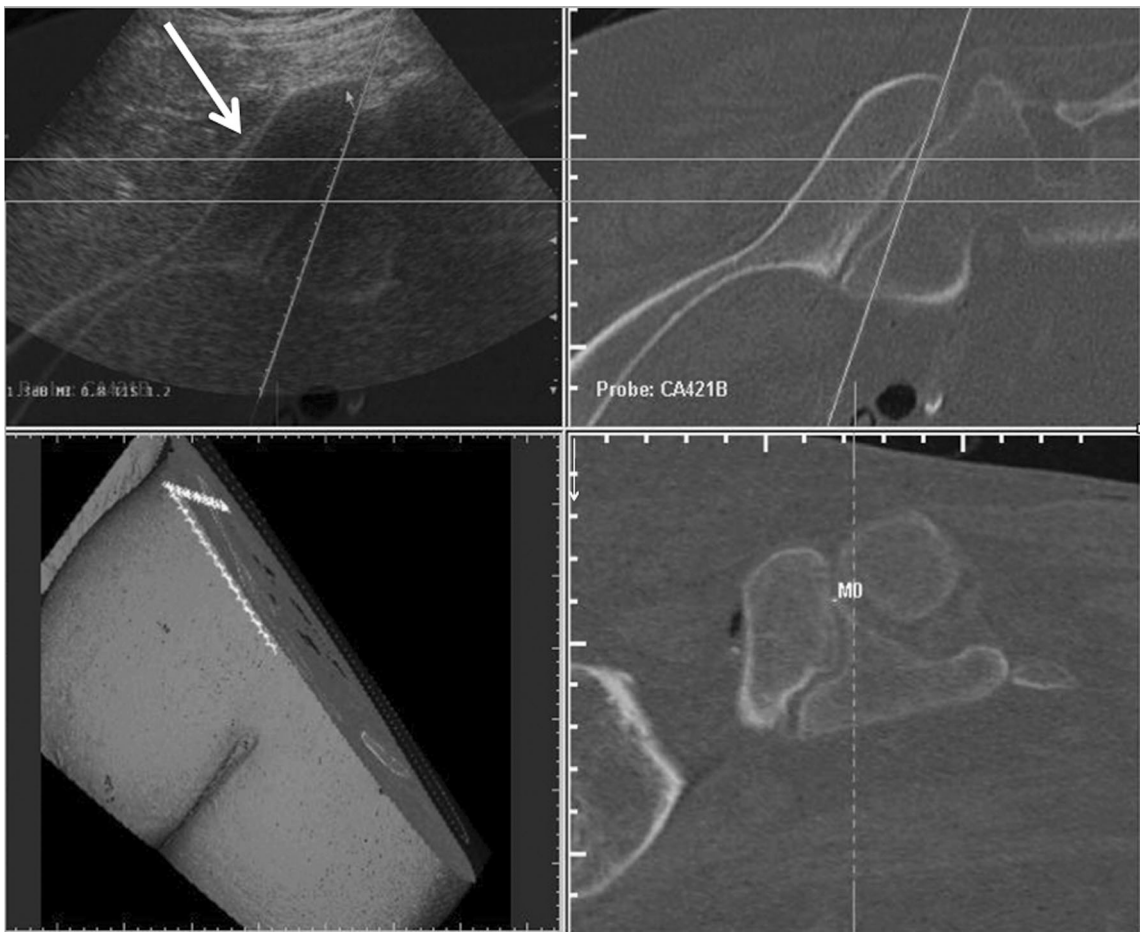

Fig. 8 US and CT fusion images. There is accurate overlapping of CT and US images of the upper right sacroiliac joint with hyperdense cortex on CT and hyperechoic cortex on US images (*arrow*), which is the first step to choose correct point of needle insertion, which will be completed by definition of M0 in all planes (example *right bottom*). US was performed on US machine (CA431, My- Lab90; Esaote Biomedica, Genoa, Italy) with a 1–8-MHz curved-array transducer. M0 represents the first placed marker in order to allow for fusion of CT with US; the second placed marker would display as M1 and so on. It is possible to place as many markers as necessary to allow for the best fit of overlapping both imaging modalities when performing real-time US

Similar relationships could not be detected with thickness ratio and cross-sectional area ratio. [36].

Shinohara and collaborators studied the distribution of local gastrocnemius muscle stiffness within and between resting and contracting muscles of different lengths using a high frame rate (5 kHz) SWE US technique on the Aixplorer machine (Aixplorer; SuperSonic Imagine, Aix-en-Provence, France) with an 8-MHz linear array transducer. Quantitative elastography maps were used to display the results from normal muscles at rest or contraction in kilopascals. The Young modulus of the gastrocnemius muscle was 16.5 kPa at rest and 225.4 kPa during contraction, of the soleus 14.5 kPa at rest and 55.0 kPa during contraction and of the tibialis anterior was 40.6 kPa at rest and 268.2 kPa during contraction by using SWE with increased stiffness upon contraction. The authors concluded that this technique may assist clinicians in characterizing muscle injuries or neuromuscular disorders [37].

In their recent study, Wang et al. developed a dynamic vibro-ultrasound system to measure SWE of the lower leg using the SonixRP (Ultrasonix Medical Corp. Vancouver, Canada) commercial ultrasound system and 10 MHz linear array. The system was used to assess stiffness of the vastus intermedius muscle of ten healthy elderly female subjects and ten healthy young female subjects. The stiffness of the vastus intermedius muscle positively correlated to the percent of maximum voluntary contraction level over the entire range of isometric contraction (from 0 to 100 %). There was no significant difference between the mean vastus intermedius shear modulus between the elderly and young subjects in a relaxed state. However, a significant difference was found with isometric contraction, with the stiffness of the vastus intermedius muscle of young female subjects larger than that of elderly participants, especially with larger contractions [38].

Lacourpaille and collaborators performed SWE on 14 patients with Duchenne muscular dystrophy (DMD) and 13

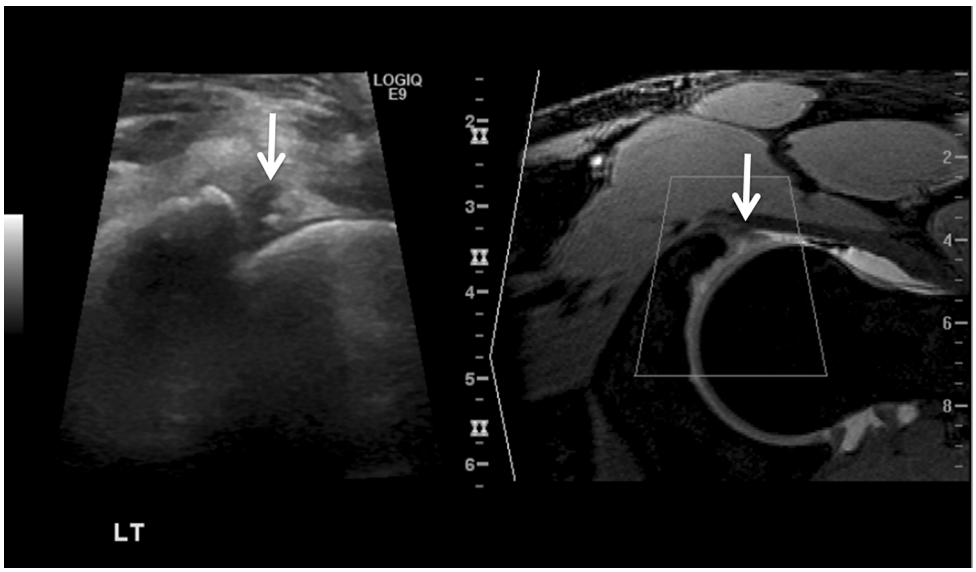

Fig. 9 US and MR fusion images. Axial oblique grayscale and MR arthrogram fusion images of the hip show hypoechoic area undercutting the anterior acetabular labrum on the US image (on the *left*) with intrarticular contrast undercutting the acetabular labrum on the MR arthrogram image (on the *right*) consistent with labral tear. Courtesy of Marnix Van Holsbeeck MD, Detroit, MI, USA

control subjects. Six muscles were measured at two muscle lengths (shortened and stretched) including the medial head of gastrocnemius, tibialis anterior, vastus lateralis, and several additional muscles of the upper extremity. An US machine (Aixplorer; Supersonic Imagine, France) coupled with a linear transducer array (4-15 MHz) was used in SWE mode. The study revealed significantly higher stiffness in DMD patients compared to controls for all the muscles suggesting that SWE is a sensitive non-invasive technique to assess the increase in muscle stiffness associated with DMD [39•].

There are no clinical studies employing SWE on the peripheral nerves of the lower extremity. A recent SWE study compared median nerve stiffness at the carpal tunnel in 37 consecutive patients (60 wrists) with a definitive diagnosis of carpal tunnel syndrome and in 18 healthy volunteers (36 wrists) with promising results. The US examinations were performed using a 15-4-MHz linear array transducer on an Aixplorer US machine (Aixplorer; SuperSonic Imagine, France). In this study, the median nerve stiffness was significantly higher in the patient group than in the control group, and higher in those with more severe disease than with milder disease [40].

There is interest for using SEL with ARFI to improve conventional US guidance in regional anesthesia procedures. In an experimental cadaveric study and subsequent in vivo human study performed on two healthy male subjects before, during and after saline injections, images revealed improved SEL contrast over B-mode in visualization of the sciatic nerve and surrounding tissues. Peripheral nerves are surrounded by other anatomic structures with different viscoelastic properties that can provide a mechanical basis for improved elasticity-based image contrast when acoustic B-mode contrast is limited. In this study, SEL using ARFI enabled up to 600 % contrast improvement in large distal lower limb nerves. However, the authors concluded that additional comprehensive studies are needed to evaluate for feasibility of concurrent use of B-mode and ARFI US images to facilitate regional anesthesia procedures [41].

A few clinical studies were published investigating SEL of the soft tissues of the lower extremity using an external vibrator [42, 43].

In the study by Aubry and collaborators using a Rubi V1Sq (Supersonic Imagine), the mean Young's modulus of the Achilles tendon at three different levels of plantar flexion with use of TE was 104 kPa during extension, 464 kPa in the neutral position, and 410 kPa during maximum dorsiflexion in the longitudinal plane [42].

Nordez and collaborators performed SEL to measure local muscle hardness of the medial head of the gastrocnemius muscle belly in ten subjects during passive ankle stretching. The local hardness of the medial head of gastrocnemius muscle belly showed a positive correlation with the passive stretching with no significant change in the resting position 10 min after stretching, indicating that changes in passive torque following static stretching could be explained by an acute increase in muscle length without any changes in intrinsic mechanical musculo-articular properties [43].

US Fusion Imaging

There are several advantages of fusing the real-time US imaging with imported pre-existing CT or MR images. Klauser and collaborators reported promising results with fusing real-time US with CT images to facilitate the injection of the sacroiliac joints, which was initially

performed in ten cadaveric specimens, and subsequently in ten sacroiliac joints in seven patients [44]. Figure 8 shows an example of US/CT imaging fusion of the sacroiliac joint. In a recent study, Vollman and collaborators emphasized the value of fusion US and MR images in teaching radiology residents US anatomy [45•]. Figure 9 shows correlative US/MR imaging anatomy of the hip joint. Further studies on fusion of the US studies with the other imaging modalities are awaited.

Conclusion

Musculoskeletal US is a rapidly evolving imaging modality, which is increasingly being used in everyday clinical practice and innovative research protocols. SEL may increase diagnostic accuracy by providing additional information regarding tissue elasticity with SWE enabling quantitative assessment. Further development of three-dimensional SEL may help in volumetric assessment of the examined tissues. Fusion of the real-time US images with CT and MR images may facilitate performing the US-guided procedures and help in teaching anatomy of the musculoskeletal system.

Compliance with Ethics Guidelines

Conflict of Interest Dr. Mihra S. Taljanovic, Dr. David M. Melville, Dr. Andrea Sabine Klauser, Dr. Hina Arif-Tiwari, Dr. Liang Gao, and Dr. Russell S. Witte each declare no potential conflicts of interest. Dr. Leonard Daniel Latt reports Grants from Orthopaedic Research and Education Foundation.

Human and Animal Rights and Informed Consent This article does not contain any studies with human or animal subjects performed by any of the authors.

References

Recently published papers of particular interest have been highlighted as:

- Of importance

1. Jacobson JA. Musculoskeletal ultrasound: focused impact on MRI. Am J Roentgenol. 2009;193(3):619–27.
2. Bracken J, Ditchfield M. Ultrasonography in developmental dysplasia of the hip: what have we learned? Pediatr Radiol. 2012;42(12):1418–31. doi:10.1007/s00247-012-2429-8.
3. Royall NA, Farrin E, Bahner DP, Stawicki SP. Ultrasound-assisted musculoskeletal procedures: a practical overview of current literature. World J Orthop. 2011;2(7):57–66. doi:10.5312/wjo.v2.i7.
4. Robotti G, Canepa MG, Bortolotto C, Draghi F. Interventional musculoskeletal US: an update on materials and methods. J Ultrasound. 2013;16(2):45–55. doi:10.1007/s40477-013-0018-9.
5. James SL, Ali K, Pocock C, Robertson C, Walter J, Bell J, et al. Ultrasound guided dry needling and autologous blood injection for patellar tendinosis. Br J Sports Med. 2007;41(8):518–21 (discussion 522).
6. de Vos RJ, Weir A, van Schie HT, Bierma-Zeinstra SM, Verhaar JA, Weinans H, et al. Platelet-rich plasma injection for chronic Achilles tendinopathy: a randomized controlled trial. JAMA. 2010;303(2):144–9.
7. Lee KS, Rosas HG, Phancao JP. Snapping hip: imaging and treatment. Semin Musculoskelet Radiol. 2013;17(3):286–94. doi:10.1055/s-0033-1348095.
8. Lewis CL. Extra-articular snapping hip: a literature review. Sports Health. 2010;2(3):186–90.
9. Garbuz DS, Hargreaves BA, Duncan CP, Masri BA, Wilson DR, Forster BB. The John Charnley award: diagnostic accuracy of MRI versus ultrasound for detecting pseudotumors in asymptomatic metal-on-metal THA. Clin Orthop Relat Res. 2014;472(2):417–23. doi:10.1007/s11999-013-3181-6.
10. Nishii T, Sakai T, Takao M, Yoshikawa H, Sugano N. Ultrasound screening of periarticular soft tissue abnormality around metal-on-metal bearings. J Arthroplast. 2012;27(6):895–900. doi:10.1016/j.arth.2011.09.015.
11. Teh J. Applications of Doppler imaging in the musculoskeletal system. Curr Probl Diagn Radiol. 2006;35(1):22–34.
12. Klauser AS, Miyamoto H, Bellmann-Weiler R, Feuchtner GM, Wick MC, Jaschke WR. Sonoelastography: musculoskeletal applications. Radiology. 2014;272(3):622–33. doi:10.1148/radiol.14121765.
13. Drakonaki EE, Allen GM, Wilson DJ. Ultrasound elastography for musculoskeletal applications. Br J Radiol. 2012;85(1019):1435–45. doi:10.1259/bjr/93042867.
14. Ophir J, Céspedes I, Ponnekanti H, Yazdi Y, Li X. Elastography: a quantitative method for imaging the elasticity of biological tissues. Ultrason Imaging. 1991;13(2):111–34.
15. Ponnekanti H, Ophir J, Huang Y, Céspedes I. Fundamental mechanical limitations on the visualization of elasticity contrast in elastography. Ultrasound Med Biol. 1995;21(4):533–43.
16. Ophir J, Alam SK, Garra BS, et al. Elastography: imaging the elastic properties of soft tissues with ultrasound. J Med Ultrason. 2002;29(4):155–71.
17. Klauser AS, Tagliafico A, Allen GM, et al. Clinical indications for musculoskeletal ultrasound: a Delphi-based consensus paper of the European Society of Musculoskeletal Radiology. Eur Radiol. 2012;22(5):1140–8.
18. Klauser AS, Faschingbauer R, Jaschke WR. Is sonoelastography of value in assessing tendons? Semin Musculoskelet Radiol. 2010;14(3):323–33.
19. • Gao L, Yuan JS, Heden GJ, Szivek JA, Taljanovic MS, Latt LD, Witte RS. Ultrasound elasticity imaging for determining the mechanical properties of human posterior tibial tendon: a cadaveric study. IEEE Trans Biomed Eng. 2014. doi:10.1109/TBME.2014.2381002. *The authors measure Young's modulus of 5 human cadaveric posterior tibial tendons using tension elastography. Although this technique is not yet commercially available, it holds great promise as a new functional imaging test of tendon, which may help guide treatment for degenerative disease of tendons.*
20. Bercoff J, Tanter M, Fink M. Supersonic shear imaging: a new technique for soft tissue elasticity mapping. IEEE Trans Ultrason Ferroelectr Freq Control. 2004;51(4):396–409.
21. Li Y, Snedeker JG. Elastography: modality-specific approaches, clinical applications, and research horizons. Skelet Radiol. 2011;40(4):389–97. doi:10.1007/s00256-010-0918-0.
22. De Zordo T, Chhem R, Smekal V, Feuchtner G, Reindl M, Fink C, Faschingbauer R, Jaschke W, Klauser AS. Real-time sonoelastography: findings in patients with symptomatic achilles

tendons and comparison to healthy volunteers. Ultraschall Med. 2010;31(4):394–400. doi:10.1055/s-0028-1109809.
23. De Zordo T, Fink C, Feuchtner GM, Smekal V, Reindl M, Klauser AS. Real-time sonoelastography findings in healthy Achilles tendons. Am J Roentgenol. 2009;193(2):W134–8. doi:10.2214/AJR.08.1843.
24. Drakonaki EE, Allen GM, Wilson DJ. Real-time ultrasound elastography of the normal Achilles tendon: reproducibility and pattern description. Clin Radiol. 2009;64(12):1196–202. doi:10.1016/j.crad.2009.08.006.
25. Tan S, Kudaş S, Özcan AS, İpek A, Karaoğlanoğlu M, Arslan H, Bozkurt M. Real-time sonoelastography of the Achilles tendon: pattern description in healthy subjects and patients with surgically repaired complete ruptures. Skelet Radiol. 2012;41(9):1067–72. doi:10.1007/s00256-011-1339-4.
26. Klauser AS, Miyamoto H, Tamegger M, et al. Achilles tendon assessed with sonoelastography: histologic agreement. Radiology. 2013;267(3):837–42.
27. Rist HJ, Mauch M. Quantified TDI elastography of the patellar tendon in athletes (in German). Sportverletz Sportschaden. 2012;26(1):27–32.
28. Wu CH, Chang KV, Mio S, Chen WS, Wang TG. Sonoelastography of the plantar fascia. Radiology. 2011;259(2):502–7.
29. Drakonaki EE, Allen GM. Magnetic resonance imaging, ultrasound and real-time ultrasound elastography of the thigh muscles in congenital muscle dystrophy. Skelet Radiol. 2010;39(4):391–6.
30. Vasilescu D, Vasilescu D, Dudea S, BotarJid C, Sfrângeu S, Cosma D. Sonoelastography contribution in cerebral palsy spasticity treatment assessment, preliminary report: a systematic review of the literature apropos of seven patients. Med Ultrasound. 2010;12(4):306–10.
31. Cantisani V, Orsogna N, Porfiri A, Fioravanti C, D'Ambrosio F. Elastographic and contrast-enhanced ultrasound features of a benign schwannoma of the common fibular nerve. J Ultrasound. 2013;16(3):135–8. doi:10.1007/s40477-013-0027-8.
32. Arda K, Ciledag N, Aktas E, Aribas BK, Köse K. Quantitative assessment of normal soft-tissue elasticity using shear-wave ultrasound elastography. Am J Roentgenol. 2011;197(3):532–6.
33. • DeWall RJ, Slane LC, Lee KS, Thelen DG. Spatial variations in Achilles tendon shear wave speed. J Biomech. 2014;47(11):2685–2692. doi: 10.1016/j.jbiomech.2014.05.008. *The results of this study showed that shear wave speed is closely linked to the spatial position along the Achilles tendon, varies between the medial and lateral sides, and depends directly on ankle posture. These observations demonstrated the critical importance of considering both spatial location and posture when using SWE for biomechanical or clinical evaluations of the Achilles tendon.*
34. Chen XM, Cui LG, He P, Shen WW, Qian YJ, Wang JR. Shear wave elastographic characterization of normal and torn achilles tendons: a pilot study. J Ultrasound Med. 2013;32(3):449–55.
35. Aubry S, Nueffer JP, Tanter M, Becce F, Vidal C, Michel F. Viscoelasticity in achilles tendonopathy: quantitative assessment by using real-time shear-wave elastography. Radiology. 2015;274(3):821–9. doi:10.1148/radiol.14140434.
36. Zhang ZJ, Ng GY, Lee WC, Fu SN. Changes in morphological and elastic properties of patellar tendon in athletes with unilateral patellar tendinopathy and their relationships with pain and functional disability. PLoS One. 2014;9(10):e108337. doi:10.1371/journal.pone.0108337.
37. Shinohara M, Sabra K, Gennisson JL, Fink M, Tanter M. Real-time visualization of muscle stiffness distribution with ultrasound shear wave imaging during muscle contraction. Muscle Nerve. 2010;42(3):438–41.
38. Wang CZ, Li TJ, Zheng YP. Shear modulus estimation on vastus intermedius of elderly and young females over the entire range of isometric contraction. PLoS One. 2014;9(7):e101769. doi:10.1371/journal.pone.0101769.
39. • Lacourpaille L, Hug F, Guével A, Péréon Y, Magot A, Hogrel JY, Nordez A. Non-invasive assessment of muscle stiffness in patients with duchenne muscular dystrophy. Muscle Nerve. 2014. doi: 10.1002/mus.24445. *The study revealed significantly higher stiffness in DMD patients compared to controls for all the muscles suggesting that SWE is a sensitive non-invasive technique to assess the increase in muscle stiffness associated with DMD.*
40. Kantarci F, Ustabasioglu FE, Delil S, Olgun DC, Korkmazer B, Dikici AS, Tutar O, Nalbantoglu M, Uzun N, Mihmanli I. Median nerve stiffness measurement by shear wave elastography: a potential sonographic method in the diagnosis of carpal tunnel syndrome. Eur Radiol. 2014;24(2):434–40. doi:10.1007/s00330-013-3023-7.
41. Palmeri ML, Dahl JJ, MacLeod DB, Grant SA, Nightingale KR. On the feasibility of imaging peripheral nerves using acoustic radiation force impulse imaging. Ultrason Imaging. 2009;31(3):172–82.
42. Aubry S, Risson JR, Barbier-Brion B, Tatu L, Vidal C, Kastler B. Transient elastography of calcaneal tendon: preliminary results and future prospects (in French). J Radiol. 2011;92(5):421–7.
43. Nordez A, Gennisson JL, Casari P, Catheline S, Cornu C. Characterization of muscle belly elastic properties during passive stretching using transient elastography. J Biomech. 2008;41(10):2305–11.
44. Klauser AS, De Zordo T, Feuchtner GM, Djedovic G, Weiler RB, Faschingbauer R, Schirmer M, Moriggl B. Fusion of real-time US with CT images to guide sacroiliac joint injection in vitro and in vivo. Radiology. 2010;256(2):547–53. doi:10.1148/radiol.10090968.
45. • Vollman A, Hulen R, Dulchavsky S, Pinchcofsky H, Amponsah D, Jacobsen G, Dulchavsky A, van Holsbeeck M. Educational benefits of fusing magnetic resonance imaging with sonograms. J Clin Ultrasound. 2014;42(5):257–263. doi: 10.1002/jcu.22136. *The authors emphasized the value of fusion US and MR images in teaching radiology residents US anatomy.*